Title: Total Synthesis of Himastatin

Authors: Kyan A. D'Angelo[1], Carly K. Schissel[1], Bradley L. Pentelute[1*], Mohammad Movassaghi[1*]

Affiliations:

[1] Department of Chemistry, Massachusetts Institute of Technology, Cambridge, Massachusetts 02139, United States

*Corresponding authors. Email: movassag@mit.edu, blp@mit.edu

Abstract: The synthesis and study of antibiotic natural products with unique structures and mechanisms of action represents a proven strategy to combat the public health crisis posed by antibiotic-resistant bacteria. The natural product himastatin is an antibiotic with an unusual homodimeric structure that presents a significant synthetic challenge. We report the concise total synthesis of himastatin by a newly developed final-stage dimerization strategy that was inspired by a detailed consideration of its biogenesis. Combining our bio-inspired dimerization approach with a modular synthesis enabled expedient access to a number of designed derivatives of himastatin, including synthetic probes that provide insight into its antibiotic activity.

Main Text:

The proliferation of multi-drug resistant pathogenic bacteria is widely recognized as an eminent threat to global health (*1,2*). Since their discovery, natural products have served as the primary inspiration for new antibiotics to treat bacterial infections (*3*). (–)-Himastatin (**1**) is a macrocyclic peptide antibiotic with a homodimeric structure isolated from *Streptomyces himastatinicus* (Fig. 1) (*4,5,6*). While (–)-himastatin's (**1**) mechanism of action is not known, an early investigation demonstrated that its antibiotic activity was reduced in the presence of sodium salts of phospholipids and fatty acids, leading to speculation that (–)-himastatin (**1**) may target the bacterial membrane (*7*). The first member discovered in this family (Fig. S1), (–)-himastatin's (**1**) homodimeric structure does not show resemblance to any well-characterized antibiotic class, including known membrane-disrupting cyclic peptides. The most striking structural feature of (–)-himastatin (**1**) is the central C5–C5' linkage between cyclotryptophan residues that is formed in the final biosynthetic step (*8*) and is critical for the observed Gram-positive antibiotic activity (*9*). Related monomeric natural products, including NW-G01 (**S2**), show a significant enhancement in antibiotic activity upon enzymatic dimerization (*10*). Other notable structural features of (–)-himastatin (**1**) include the alternating sequence of D- and L-amino acids, a depsipeptide linkage, and the piperazic acid residue with γ-hydroxylation.

Danishefsky's landmark synthesis of (–)-himastatin (**1**), which clarified the Cα stereochemistry of the cyclotryptophan residue, featured an early-stage Stille coupling to form the central C5−C5' linkage followed by bidirectional elaboration of a dimeric cyclotryptophan (*9*). Early-stage formation of this linkage was also utilized in total syntheses of the related natural product (–)-chloptosin (**S1**) by Yao (*11*) and Ley (*12*), who found that cross-coupling approaches to achieve a more attractive late-stage dimerization that would offer access to heterodimeric derivatives were not successful (*12*). Motivated by the unique structure, established synthetic challenge, and antibiotic activity, we became interested in developing a concise total synthesis of (–)-himastatin (**1**) that would offer rapid access to novel derivatives for chemical biology studies.

The key unaddressed challenge of uniting two complex fragments to form the C5−C5' bond at the center of (–)-himastatin's (**1**) dimeric structure encouraged us to consider the development of new synthetic methodology. To address the C_{sp2}–C_{sp2} linkage present in (–)-himastatin (**1**), we needed to

identify a new strategy that stands apart from our group's prior radical-based approaches to secure C_{sp3}–C_{sp3} linkages and C_{sp3}–C_{sp2} linkages between similar (*13*) and dissimilar fragments (*14*). We began with a detailed examination of (–)-himastatin's (**1**) biogenesis from a linear peptide **4** that is cyclized and then subject to oxidative tailoring by three cytochrome p450 enzymes (*8*). The final step, catalyzed by HmtS, forges the central C5–C5' bond by oxidative dimerization of (+)-himastatin monomer (**2**). Based on recent theoretical studies of p450-catalyzed C–C bond formation, we envisioned that this enzymatic dimerization may take place via radical–radical coupling of two cyclotryptophan radicals (Fig. S2) (*15,16*). These radical species are likely generated in rapid succession via indoline N–H hydrogen-atom abstraction at the heme active site, before undergoing combination in its vicinity (*16,17*).

We envisioned that a biogenetically-inspired chemical method for the oxidative dimerization of cyclotryptophans could follow the same radical–radical coupling blueprint. As opposed to hydrogen atom abstraction, we planned to generate an analogous open-shell cyclotryptophan species via single-electron oxidation of the embedded aniline substructure. Consistent with studies of aniline dimerization via single-electron oxidation (*18,19*,*20*), we predicted that the resulting arylamine radical cation would rapidly dimerize at the most accessible position, forming the desired C5–C5' linkage. Late-stage application of this chemistry to dimerization of (+)-himastatin monomer (**2**) permits a straightforward modular assembly of linear hexadepsipeptide **5** akin to native precursor **4**, without the constraints imposed by bidirectional elaboration of a simple dimeric cyclotryptophan (*9*,*11,12*). Direct union of complex peptide macrocycles also offers the elusive opportunity to access the first heterodimeric derivatives of (–)-himastatin (**1**).

Our new dimerization method required the identification of a single-electron oxidant that would target the aniline substructure within a complex cyclotryptophan precursor (*21*). We discovered that stoichiometric silver(I) hexafluoroantimonate, in combination with the non-nucleophilic pyrimidine base TTBP (*22*) in 1,2-dichloroethane, could effect C5−C5' dimerization of cyclotryptophan, cyclotryptamine, and indoline derivatives (Fig. 2A). In each case, a single regioisomer consistent with a symmetric C5−C5' linked homodimer was isolated. Single crystal X-ray diffraction of dimeric *endo*-diketopiperazine (+)-**7h** verified the expected connectivity. The use of an aqueous sodium thiosulfate reductive workup was critical for optimal isolation of the products due to their sensitivity toward further oxidation under the reaction conditions (*23*,*24*). Notably, we found that *exo*-configured diketopiperazines **6e** and **6g** were subject to complete oxidation in approximately half the time of their corresponding *endo*-derivatives **6f** and **6h**, respectively. This finding correlates with the increased accessibility of the N1 locus in substrates **6e** and **6g**, the site of initial oxidation (*25*). Substitution of N1 with a methyl group in the case of indoline **6k** did not inhibit the dimerization, consistent with a radical intermediate as opposed to a closed-shell arenium cation (*26*). In order to expand the range of reagents that could be utilized in more complex applications of our dimerization method, we also investigated the use of copper(II) salts as single-electron oxidants (*20*). Cyclotryptophan dimer (–)-**7a** could be obtained using catalytic copper(II) trifluoromethanesulfonate and silver(I) carbonate as the terminal oxidant, albeit in lower yield (34%, 18% RSM) compared to stoichiometric $AgSbF_6$ (54%).

To investigate the mechanism of this C−C bond forming dimerization reaction, we devised a series of experiments using indoline substrates (Figs. 2B and S3) (*23*). When an equimolar mixture of C2-methyl and C2-phenyl indolines **6i** and **6j**, respectively, were subjected to our dimerization conditions, we observed a statistical mixture of homo- and heterodimers that arise from similar rates of single-electron oxidation (Fig. 2B, green; Fig. S3, eq. 1). However, oxidative dimerization of an equal mixture of indolines **6j** and **6k** gave predominant (90%) homodimer formation, along with a trace (4%) amount of heterodimer **7n** (Fig. S3, eq. 2). When a limiting quantity of oxidant was used, we determined that these indoline substrates were consumed sequentially, with N1-methyl indoline **6k** dimerizing selectively over NH indoline **6j** (Fig. 2B, blue; Fig. S3 eq. 3). Having observed homodimerization of a more readily oxidized monomer in the presence of a similarly nucleophilic but less readily oxidized monomer, we conclude that C5−C5' bond formation preferentially occurs through radical–radical coupling rather than

nucleophilic capture. This conclusion is consistent with the absence of adduct formation in the homodimerization of cyclotryptophan **6a** despite the presence of external π-nucleophiles (e.g. methallyltrimethylsilane, dimethylketene silyl acetal, *N*-trimethylsilylindoline), and is reinforced by prior studies demonstrating that radical–radical coupling between aniline radical cations is fast ($k = \sim 10^7$ $M^{-1} \bullet s^{-1}$ for the dimerization of $PhNMe_2^{\bullet+}$) (*18,19,20*). We postulate that the high local concentration of radical species near the surface of the oxidant favors their direct combination over nucleophilic pathways (*14*,*20*). In the context of our synthetic efforts, the rapid rate and apparent insensitivity of the radical–radical coupling manifold to nucleophilic interference bode well for the application of this chemistry to complex substrates. These findings highlight a possible underlying parallel between our oxidative dimerization methodology and our mechanistic proposal for the biosynthetic dimerization catalyzed by HmtS (Fig. S2), involving successive generation of radical species in close proximity to each other.

For the synthesis of (+)-himastatin monomer (**2**), we sought to leverage the practical advantages of solid-phase peptide synthesis (*27*), offering rapid and customizable access to complex peptides by minimizing repetitive purification and isolation steps. In contrast to the reported solution-based approach to intermediates en route to (–)-himastatin (**1**) (*9*), we relied on a hybrid solution-solid phase synthetic strategy. The resin-bound D-threonine **9** (Fig. 3) was elaborated with L-leucine (–)-**10** and depsitripeptide fragment (+)-**8**, the latter being prepared in one step from a depsipeptide block (*28*) and known *Nε*,*O*-protected D-5-hydroxypiperazic acid (*9*). The crude depsipentapeptide acid (+)-**11** obtained upon cleavage was then coupled with cyclotryptophan (–)-**12** (Fig. S4), affording linear hexadepsipeptide (–)-**13** in 55% overall yield from threonine resin **9** (*23*). The efficient hybrid synthetic strategy we have developed enables convergent assembly of intermediate hexadepsipeptide (–)-**13** with only a single chromatographic purification, and compares favorably to linear solution-phase synthesis which requires at least 10 separate steps to access an intermediate of similar complexity (*9*). Furthermore, our modular strategy allows for conducting difficult couplings in solution (*28*), and introducing the tryptophan residue as a cyclotryptophan to bypass stereoselectivity concerns that would arise from late-stage oxidation (*29*). The resulting linear peptide (–)-**13** was cyclized to (+)-himastatin monomer (**2**) in 46% overall yield (Fig. 4), affording the immediate biosynthetic precursor to (–)-himastatin (**1**). All ^1H and ^{13}C NMR data as well as optical rotation for synthetic monomer (+)-**2** were consistent with literature values (*8*,*9*).

Having accessed (+)-himastatin monomer (**2**), we focused on the application of our biogenetically inspired oxidative dimerization methodology to complete the total synthesis of (–)-himastatin (**1**) (Fig. 3). While silver(I) hexafluoroantimonate and copper(II) trifluoromethanesulfonate were effective for the dimerization of simpler cyclotryptophans (Fig. 2), they gave little to no oxidation of the cyclotryptophan incorporated within the more complex (+)-himastatin monomer (**2**). We hypothesized that aggregation and inactivation of these insoluble oxidants, combined with the lower reactivity of complex macrocyclic peptide substrates, may be responsible for the low conversion, and sought to address the challenge posed by evaluating other single-electron oxidants. Consistent with this hypothesis, insoluble oxidants such as other Ag(I,II) and Cu(II) salts were generally ineffective. However, soluble oxidants including organic radical cations such as magic blue ($(4\text{-}BrPh)_3N^{\bullet+}SbF_6$), did provide oxidation, but products derived from nucleophilic substitution of the C–Br bond (S_NAr) by the peptide dominated (*21*). Informed by our prior use of Cu(II) for the dimerization of simpler substrates and in search of an oxidant with both good solubility and low propensity toward nucleophilic capture, we identified copper(II) hexafluoroantimonate. Our isolation of freshly prepared $Cu(SbF_6)_2$, commonly used as a soluble Lewis acid catalyst (*30*), provided us with an opportunity to investigate its use as a stoichiometric oxidant. In the event, exposure of (+)-himastatin monomer (**2**) to $Cu(SbF_6)_2$ and DTBMP in 1,2-dichloroethane, afforded (–)-himastatin (**1**) in 40% yield, with only trace (<5%) amounts of recovered starting material. All spectroscopic data, as well as optical rotation, for synthetic (–)-himastatin (**1**) were consistent with literature values (*6,9*).

Our concise and versatile chemical synthesis of himastatin, featuring a biogenetically inspired final-stage dimerization reaction, presented an opportunity both to interrogate structural characteristics that are important for its bioactivity, and to access synthetic probes for chemical biology studies (Fig. 4). We hypothesized that the alternating sequence of D,L-residues present in the macrocyclic rings of (–)-himastatin (**1**) could promote self-assembly (*31,32*), inspiring our preparation of both the enantiomer (*ent*-(+)-**1**) and *meso* derivative of himastatin (**1**). These stereochemical probes were prepared from precursors of opposite chirality, and in the case of the heterodimer *meso*-himastatin (**1**), by dimerization of an equal mixture of monomer **2** enantiomers and separation of the resulting heterodimer (*23*). Apart from slight variations in the chemical shifts of aromatic ^{1}H and ^{13}C signals, the spectra of *meso*-himastatin (**1**) were nearly identical to the corresponding homodimers. We also selected several derivatives with single-residue substitutions to synthesize, each varying a residue that is unique to himastatin amongst related antibiotics. In all cases, our modular hybrid peptide synthesis approach was quickly adapted to introduce the substituted residue, and the resulting monomers were effectively dimerized (21-37% yield) using the conditions developed for the synthesis of (–)-himastatin (**1**) (Fig. 4A) (*23*). As an orthogonal mechanistic probe that would permit direct visualization of himastatin's interaction with bacteria, we designed a fluorescent heterodimer that we predicted would retain antibiotic activity (vide infra). TAMRA-himastatin heterodimer (–)-**25** was rapidly prepared via the union of himastatin monomer (+)-**2** and azidolysine monomer (+)-**22** followed by labelling via a reduction–acylation sequence (Fig. 4B). This procedure also provided access to TAMRA-himastatin homodimer (–)-**S17** as a useful control (*23*).

We found that synthetic (–)-himastatin (**1**) showed antibiotic activity against several Gram-positive species, including antibiotic-resistant strains of public health concern (Fig. 4C, Table S10) (*1*). Our synthetic (–)-himastatin (**1**) showed similar MIC values (1–2 μg/mL) to those reported for natural (–)-himastatin (**1**) in identical species (*4*). All monomeric derivatives prepared in this study had MIC values ≥64 μg/mL across all species tested (*23*), highlighting the critical role of dimerization for antibiotic activity. Our stereochemical probes revealed that the absolute stereochemistry of himastatin has negligible impact on its antibiotic activity; stereoisomers of himastatin (**1**) were found to have nearly identical MIC values across the *B. subtilis*, *S. aureus*, and *E. faecalis* strains tested. This finding has also been observed amongst enantiomers of certain membrane-targeting cyclic peptides with alternating stereochemistry (*33*), and is consistent with antibiotic activity depending on achiral as opposed to diastereomeric interactions that would lead to differential activity of each stereoisomer (e.g. with peptides or receptors) (*34*,*35*). In contrast, we found that *ent*-(+)-himastatin (**1**) was 4–8 fold more active in inhibiting the growth of the producing organism, *Streptomyces himastatinicus*, compared to (–)-himastatin (**1**). This finding might be explained by the presence of known self-resistance mechanisms that have evolved in other species, such as enzymatic degradation and efflux, which would be expected to show differences between stereoisomers (*36*).

The introduction of a strategically positioned functional handle in (–)-himastatin (**1**) was a key goal of our derivative design that would permit introduction of a fluorescent tag. We focused on L-leucine substitution, given the natural variation of this site among related antibiotics (Fig. S1). Replacement with an *O*-methyl serine residue (L-Ser(OMe), dimer (–)-**21**), which is found in (–)-chloptosin (**S1**), had minimal impact on antibiotic activity. A similar finding was observed upon substitution with L-azidolysine (L-Lys(N_3), dimer (–)-**23**), which offered the conjugation site exploited in our synthesis of fluorescent probes. However, unlike serine and azidolysine homodimers (–)-**21** and (–)-**23**, respectively, the corresponding TAMRA-himastatin homodimer (–)-**S17** was inactive (MIC >64 μg/mL) (Fig. S5, Table S10). In addition to TAMRA, homodimeric himastatin analogues derived from other fluorophores were also found to be inactive (Fig. S5). Consistent with our expectation that minimizing the overall perturbation of himastatin's structure to only one half of the dimer may preserve antibiotic activity, we found that the MIC of TAMRA-heterodimer (–)-**25** (Fig. 4B) was indeed comparable to that of (–)-himtastatin (**1**) in *Bacilus subtilis* (6 vs. 1 μg/mL). Thus, the opportunity for heterodimer formation

offered by our biogenetically-inspired late-stage dimerization methodology was instrumental to secure access to a fluorescent himastatin probe (*37*), as well as other key derivatives including *meso*-himastatin (**1**) that would otherwise be significantly challenging to prepare using chemoenzymatic or bidirectional synthesis (*9,10*).

Other structural features specific to (–)-himastatin (**1**) include a depsipeptide linkage and 5-hydroxypiperazic acid residue. Evaluating the derivatives that we prepared to study these particular structural features, we observed a trend of decreasing antibiotic activity when the ester linkage was replaced with either a secondary amide (–)-**15** or tertiary amide (–)-**17**, consistent with the loss of a hydrogen-bond site (*38*). Furthermore, when the 5-hydroxypiperazic acid residue was replaced with a proline residue, antibiotic activity was completely abolished. While proline residues are known to induce turn formation, especially when the adjacent amino acid is of opposite α-stereochemistry, they do not exhibit a rigidifying effect as pronounced as that seen in *N*-acyl piperazic acid derivatives (*39*). Consistent with the predicted loss of rigidity upon proline substitution, NMR spectra of homodimer (–)-**19** and monomer (+)-**18** in various solvents at 23 °C revealed the presence of minor conformers not observed in the spectra of (–)-himastatin (**1**) or our other derivatives. Taken together, these results provide evidence that structural rigidity, enforced by hydrogen-bonding and conformational restriction, is important to himastatin's antimicrobial mode of action.

Confocal microscopy has been used to observe the biological effects of antibiotics on *B. subtilis*, including the first approved membrane-disrupting lipopeptide, daptomycin (*37*). We sought to use our synthetic compounds in conjunction with this experimental approach to further characterize the antibiotic activity of (–)-himastatin (**1**). Our synthetic heterodimeric probe, TAMRA-himastatin (–)-**25**, offered an opportunity to directly visualize its interaction with bacteria and monitor cellular localization. When *B. subtilis* cells were treated with TAMRA-himastatin (–)-**25**, we observed substantial accumulation in the bacterial envelope (Fig. S6A), with little to no intracellular staining seen at sub-lethal concentrations. The most intense sites of staining were observed at bacterial septa, in addition to patches of stain along sidewalls. At lethal concentrations (Fig. S6B), defects such as membrane extrusions coincided with lateral accumulation of TAMRA-himastatin (–)-**25**. These sites of curvature appear to reflect areas where the antibiotic has induced changes to membrane morphology.

The staining pattern observed with TAMRA-himastatin (–)-**25** was similar to that of the membrane stain FM4-64 with unmodified himastatin (**1**) (Fig. S7). Untreated *B. subtilis* cells have smooth membranes and normal septal rings, but cells treated with a sub-lethal concentration of either enantiomer of himastatin (**1**) display striking membrane defects, notably patches of membrane thickening. Furthermore, the observed similarity in membrane morphology between himastatin (**1**) enantiomers appears to be consistent with their similar antibiotic activity. In a separate experiment, we evaluated the timescale by which (–)-himastatin (**1**) acts on bacteria at lethal concentrations (Fig. S8). When treated with (–)-himastatin (**1**) at a concentration twice the MIC value, bacterial membranes were permeabilized within 30 minutes, as indicated by influx of the viability stain SYTOX Green.

The observations of our microscopy studies are comparable to those seen with daptomycin despite a lack of structural similarity to himastatin (*37*). The membrane defects and localization patterns observed in *B. subtilis* with unmodified (–)-himastatin (**1**) and our fluorescent himastatin derivative (–)-**25**, show resemblance to those seen with unmodified and fluorescent forms of daptomycin, respectively (*37*). Furthermore, the short timescale of membrane permeabilization following treatment with himastatin (**1**), like daptomycin, is consistent with a mode of action based on physical perturbations (*33,37*). This mode of action is distinct from other Gram-positive peptide antibiotics, such as vancomycin and teixobactin, that interfere with cell-wall biosynthesis and have longer kill times (*40*). Separately, the similarity in MIC values and cellular morphology amongst our series of synthetic himastatin stereoisomers reveals that achiral interactions, for example with the hydrophobic groups of phospholipids (*34,35*), are largely responsible for the observed antibiotic activity. In summary, our chemical biology studies using our

synthetic probes offer findings that are consistent with the hypothesis that (–)-himastatin's (**1**) antibiotic activity is dependent on interaction with bacterial membranes (*7*). It is evident that (–)-himastatin (**1**) is a structurally unique member amongst known membrane-disruptors. These antibiotics target an essential bacterial organelle that can be difficult to alter without severe fitness cost (*41*).

As society continues to battle multidrug-resistant pathogens, membrane-disrupting antibiotics, like the FDA-approved daptomycin, represent an important frontier in the fight. Our bioinspired strategy for the total synthesis of (–)-himastatin (**1**) provides rapid access to derivatives and is enabling investigations that point to its antibiotic activity via membrane disruption. This effort aims to facilitate further inquiries to advance our understanding and exploit how himastatin's unique molecular structure contributes to its antibiotic activity.

References and Notes

[1] H. W. Boucher, G. H. Talbot, J. S. Bradley, J. E. Edwards, D. Gilbert, L. B. Rice, M. Scheld, B. Spellberg, J. Bartlett, Bad bugs, no drugs: no ESKAPE! An update from the Infectious Diseases Society of America. *Clin. Infect. Dis.* **48**, 1–12 (2009).

[2] C. L. Ventola, The antibiotic resistance crisis: part 1: causes and threats. *Pharm. Ther.* **40**, 277–283 (2015).

[3] G. D. Wright, Something old, something new: revisiting natural products in antibiotic drug discovery. *Can. J. Microbiol.* **60**, 147–154 (2014).

[4] K. S. Lam, G. A. Hesler, J. M. Mattei, S. W. Mamber, S. Forenza, K. Tomita, Himastatin, a new antitumor antibiotic from *Streptomyces hygroscopicus*. I. Taxonomy of producing organism, fermentation and biological activity. *J. Antibiot.* **43**, 956–960 (1990).

[5] J. E. Leet, D. R. Schroeder, B. S. Krishnan, J. A. Matson, Himastatin, a new antitumor antibiotic from *Streptomyces hygroscopicus*. II. Isolation and characterization. *J. Antibiot.* **43**, 961–966 (1990).

[6] J. E. Leet, D. R. Schroeder, J. Golik, J. A. Matson, T. W. Doyle, K. S. Lam, S. E. Hill, M. S. Lee, J. L. Whitney, B. S. Krishnan, Himastatin, a new antitumor antibiotic from *Streptomyces hygroscopicus*. III. Structural elucidation. *J. Antibiot.* **49**, 299–311 (1996).

[7] S. W. Mamber, K. W. Brookshire, B. J. Dean, R. A. Firestone, J. E. Leet, J. A. Matson, S. Forenza, Inhibition of antibacterial activity of himastatin, a new antitumor antibiotic from *Streptomyces hygroscopicus*, by fatty acid sodium salts. *Antimicrob. Agents Chemother.* **38**, 2633–2642 (1994).

[8] J. Ma, Z. Wang, H. Huang, M. Luo, D. Zuo, B. Wang, A. Sun, Y.-Q. Cheng, C. Zhang, J. Ju, Biosynthesis of himastatin: assembly line and characterization of three cytochrome p450 enzymes involved in the post-tailoring oxidative steps. *Angew. Chem. Int. Ed.* **50**, 7797–7802 (2011).

[9] T. M. Kamenecka, S. J. Danishefsky, Discovery through total synthesis: a retrospective on the himastatin problem. *Chem. Eur. J.* **7**, 41–63 (2001).

[10] Z. Guo, P. Li, G. Chen, C. Li, Z. Cao, Y. Zhang, J. Ren, H. Xiang, S. Lin, J. Ju, Y. Chen, Design and biosynthesis of dimeric alboflavusins with biaryl linkages via regiospecific C–C bond coupling. *J. Am. Chem. Soc.* **140**, 18009–18015 (2018).

[11] S.-M. Yu, W.-X. Hong, Y. Wu, C.-L. Zhong, Z.-J. Yao, Total synthesis of chloptosin, a potent apoptosis-inducing cyclopeptide. *Org. Lett.* **12**, 1124–1127 (2010).

[12] A. J. Oelke, F. Antonietti, L. Bertone, P. B. Cranwell, D. J. France, R. J. M. Goss, T. Hofmann, S. Knauer, S. J. Moss, P. C. Skelton, R. M. Turner, G. Wuitschik, S. V. Ley, Total synthesis of chloptosin: a dimeric cyclohexapeptide. *Chem. Eur. J.* **17**, 4183–4194 (2011).

[13] J. Kim, J. A. Ashenhurst, M. Movassaghi, Total synthesis of (+)-11,11'-dideoxyverticillin A. *Science*. **324**, 238–241 (2009).

[14] M. Movassaghi, O. K. Ahmad, S. P. Lathrop, Directed heterodimerization: stereocontrolled assembly via solvent-caged unsymmetrical diazene fragmentation. *J. Am. Chem. Soc.* **133**, 13002–13005 (2011).
[15] J. M. Grandner, R. A. Cacho, Y. Tang, K. N. Houk, Mechanism of the p450-catalyzed oxidative cyclization in the biosynthesis of griseofulvin. *ACS Catal.* **6**, 4506–4511 (2016).
[16] R. H. Takahashi, J. M. Grandner, S. Bobba, Y. Liu, P. Beroza, D. Zhang, S. Ma, Novel homodimer metabolites of GDC-0994 via cytochrome p450–catalyzed radical coupling. *Drug. Metab. Dispos.* **48**, 521–527 (2020).
[17] V. V. Shende, Y. Khatri, S. A. Newmister, J. N. Sanders, P. Lindovska, F. Yu, T. J. Doyon, J. Kim, K. N. Houk, M. Movassaghi, D. H. Sherman, Structure and function of NzeB, a versatile C–C and C–N bond-forming diketopiperazine dimerase. *J. Am. Chem. Soc.* **142**, 17413–17424 (2020).
[18] D. Larumbe, I. Gallardo, C. P. Andrieux, Anodic oxidation of some tertiary amines. *J. Electroanal. Chem.* **304**, 241–247 (1991).
[19] H. Yang, D. O. Wipf, A. J. Bard, Application of rapid scan cyclic voltammetry to a study of the oxidation and dimerization of *N,N*-dimethylaniline in acetonitrile. *J. Electroanal. Chem.* **331**, 913–924 (1992).
[20] M. Kirchgessner, K. Sreenath, K. R. Gopidas, Understanding reactivity patterns of the dialkylaniline radical cation. *J. Org. Chem.* **71**, 9849–9852 (2006).
[21] N. G. Connelly, W. E. Geiger, Chemical redox agents for organometallic chemistry. *Chem. Rev.* **96**, 877–910 (1996).
[22] D. Crich, M. Smith, Q. Yao, J. Picione, 2,4,6-Tri-*tert*-butylpyrimidine (TTBP): a cost effective, readily available alternative to the hindered base 2,6-di-*tert*-butylpyridine and its 4-substituted derivatives in glycosylation and other reactions. *Synthesis*, 323–326 (2001).
[23] See supplementary materials.
[24] O. Ivashenko, J. T. van Herpt, P. Rudolf, B. L. Feringa, W. R. Browne, Oxidative electrochemical aryl C–C coupling of spiropyrans. *Chem. Commun.* **49**, 6737–6739 (2013).
[25] B. M. Nelson, R. P. Loach, S. Schiesser, M. Movassaghi, Concise total synthesis of (+)-asperazine A and (+)-pestalazine B. *Org. Biomol. Chem.* **16**, 202–207 (2018).
[26] P. G. Gassman, G. A. Campbell, R. C. Frederick, Nucleophilic aromatic substitution of anilines *via* aryl nitrenium ions (anilenium ions). *J. Am. Chem. Soc.* **94**, 3884–3891 (1972).
[27] J. S. Albin, B. L. Pentelute, Efficient flow synthesis of human antimicrobial peptides. *Aust. J. Chem.* **73**, 380 (2020).
[28] M. M. Nguyen, N. Ong, L. Suggs, A general solid phase method for the synthesis of depsipeptides. *Org. Biomol. Chem.* **11**, 1167–1170 (2013).
[29] K. L. Greenman, D. M. Hach, D. L. Van Vranken, Synthesis of Phakellistatin 13 and Oxidation to Phakellistatin 3 and Isophakellistatin 3. *Org. Lett.* **6**, 1713–1716 (2004).
[30] S.-K. Chang, P. Selvaraj, "Copper(II) Hexafluoroantimonate" in *Encyclopedia of Reagents for Organic Synthesis* (Wiley, 2005).
[31] P. De Santis, S. Morosetti, R. Rizzo, Conformational analysis of regular enantiomeric sequences. *Macromolecules*. **7**, 52–58 (1974).
[32] L. Tomasic, G. P. Lorenzi, Some cyclic oligopeptides with S_{2n} symmetry. *Helv. Chim. Acta*. **70**, 1012–1016 (1987).
[33] S. Fernandez-Lopez, H.-S. Kim, E. C. Choi, M. Delgado, J. R. Granja, A. Khasanov, K. Kraehenbuehl, G. Long, D. A. Weinberger, K. M. Wilcoxen, M. R. Ghadiri, Antibacterial agents based on the cyclic D,L-α-peptide architecture. **412**, 4 (2001).
[34] D. Wade, A. Boman, B. Wåhlin, C. M. Drain, D. Andreu, H. G. Boman, R. B. Merrifield, All-D amino acid-containing channel-forming antibiotic peptides. *Proc. Natl. Acad. Sci.* **87**, 4761–4765 (1990).

[35] C. K. Wang, G. J. King, A. C. Conibear, M. C. Ramos, S. Chaousis, S. T. Henriques, D. J. Craik, Mirror images of antimicrobial peptides provide reflections on their functions and amyloidogenic properties. *J. Am. Chem. Soc.* **138**, 5706–5713 (2016).
[36] E. Peterson, P. Kaur, Antibiotic Resistance Mechanisms in Bacteria: Relationships Between Resistance Determinants of Antibiotic Producers, Environmental Bacteria, and Clinical Pathogens. *Front. Microbiol.* **9**, 2928 (2018).
[37] J. Pogliano, N. Pogliano, J. A. Silverman, Daptomycin-mediated reorganization of membrane architecture causes mislocalization of essential cell division proteins. *J. Bacteriol.* **194**, 4494–4504 (2012).
[38] Y. Li, N. P. Lavey, J. A. Coker, J. E. Knobbe, D. C. Truong, H. Yu, Y.-S. Lin, S. L. Nimmo, A. S. Duerfeldt, Consequences of depsipeptide substitution on the ClpP activation activity of antibacterial acyldepsipeptides. *ACS Med. Chem. Lett.* **8**, 1171–1176 (2017).
[39] N. Xi, L. B. Alemany, M. A. Ciufolini, Elevated conformational rigidity in dipeptides incorporating piperazic acid derivatives. *J. Am. Chem. Soc.* **120**, 80–86 (1998).
[40] L. L. Ling, T. Schneider, A. J. Peoples, A. L. Spoering, I. Engels, B. P. Conlon, A. Mueller, T. F. Schäberle, D. E. Hughes, S. Epstein, M. Jones, L. Lazarides, V. A. Steadman, D. R. Cohen, C. R. Felix, K. A. Fetterman, W. P. Millett, A. G. Nitti, A. M. Zullo, C. Chen, K. Lewis, A new antibiotic kills pathogens without detectable resistance. *Nature*. **517**, 455–459 (2015).
[41] M. Roch, P. Gagetti, J. Davis, P. Ceriana, L. Errecalde, A. Corso, A. E. Rosato, Daptomycin resistance in clinical MRSA strains is associated with a high biological fitness cost. *Front Microbiol*. **8**, 2303 (2017).
[42] W. C. Still, M. Kahn, A. Mitra, Rapid chromatographic technique for preparative separations with moderate resolution. *J. Org. Chem.* **43**, 2923–2925 (1978).
[43] A. B. Pangborn, M. A. Giardello, R. H. Grubbs, R. K. Rosen, F. J. Timmers, Safe and convenient procedure for solvent purification. *Organometallics*. **15**, 1518–1520 (1996).
[44] Y. Qian, X. Xu, X. Wang, P. J. Zavalij, W. Hu, M. P. Doyle, Rhodium(II)- and copper(II)-catalyzed reactions of enol diazoacetates with nitrones: metal carbene versus Lewis acid directed pathways. *Angew. Chem. Int. Ed*. **51**, 5900–5903 (2012).
[45] H. E. Gottlieb, V. Kotlyar, A. Nudelman, NMR Chemical shifts of common laboratory solvents as trace impurities. *J. Org. Chem.* **62**, 7512–7515 (1997).
[46] C. J. Barrow, P. Cai, J. K. Snyder, D. M. Sedlock, H. H. Sun, R. Cooper, WIN 64821, a new competitive antagonist to substance P, isolated from an Aspergillus species: structure determination and solution conformation. *J. Org. Chem.* **58**, 6016–6021 (1993).
[47] R. P. Bhattacharyya, M. Walker, R. Boykin, S. S. Son, J. Liu, A. C. Hachey, P. Ma, L. Wu, K. Choi, K. C. Cummins, M. Benson, J. Skerry, H. Ryu, S. Y. Wong, M. B. Goldberg, J. Han, V. M. Pierce, L. A. Cosimi, N. Shoresh, J. Livny, J. Beechem, D. T. Hung, Rapid identification and phylogenetic classification of diverse bacterial pathogens in a multiplexed hybridization assay targeting ribosomal RNA. *Sci. Rep*. **9**, 4516 (2019).
[48] I. Wiegand, K. Hilpert, R. E. W. Hancock, Agar and broth microdilution methods to determine the minimal inhibitory concentration (MIC) of antimicrobial substances. *Nat. Protoc.* **3**, 163–175 (2008).
[49] J. S. Benco, H. A. Nienaber, W. G. McGimpsey, Synthesis of an ammonium ionophore and its application in a planar ion-selective electrode. *Anal. Chem.* **75**, 152–156 (2003).
[50] S. Eissler, M. Kley, D. Bächle, G. Loidl, T. Meier, D. Samson, Substitution determination of Fmoc-substituted resins at different wavelengths. *J. Pept. Sci.* **23**, 757–762 (2017).

Acknowledgments: We thank Wendy C. Salmon at the W. M. Keck Microscopy Facility (Whitehead Institute) for assistance with live-cell microscopy. We thank Dr. Charlene Tsay, and Dr. Peter Müller (Massachusetts Institute of Technology) for assistance with single crystal X-ray diffraction of (+)-**7h**.

We thank Dr. Roby P. Bhattacharyya (Massachusetts General Hospital) for providing several bacterial strains. We are grateful to Dr. John S. Albin (Massachusetts General Hospital) for helpful discussions.

Funding: Supported by NIH grants GM-089732 and GM-141963; the Natural Sciences and Engineering Research Council of Canada (postgraduate scholarship to K.A.D.); and an NSF graduate research fellowship 4000057398 (C.K.S.).

Author contributions: K.A.D. and M.M. conceived the project and designed the synthetic routes; K.A.D. performed the chemical synthesis; C.K.S. performed the antibiotic assays and fluorescence microscopy; all co-authors wrote and edited the manuscript.

Competing interests Authors declare that they have no competing interests.

Data and materials availability: Experimental procedures, spectroscopic data, and copies of NMR spectra are available in supplementary materials. Structural parameters for *endo*-diketopiperazine (+)-**7h** are freely available from the Cambridge Crystallographic Data Centre under CCDC-2099734.

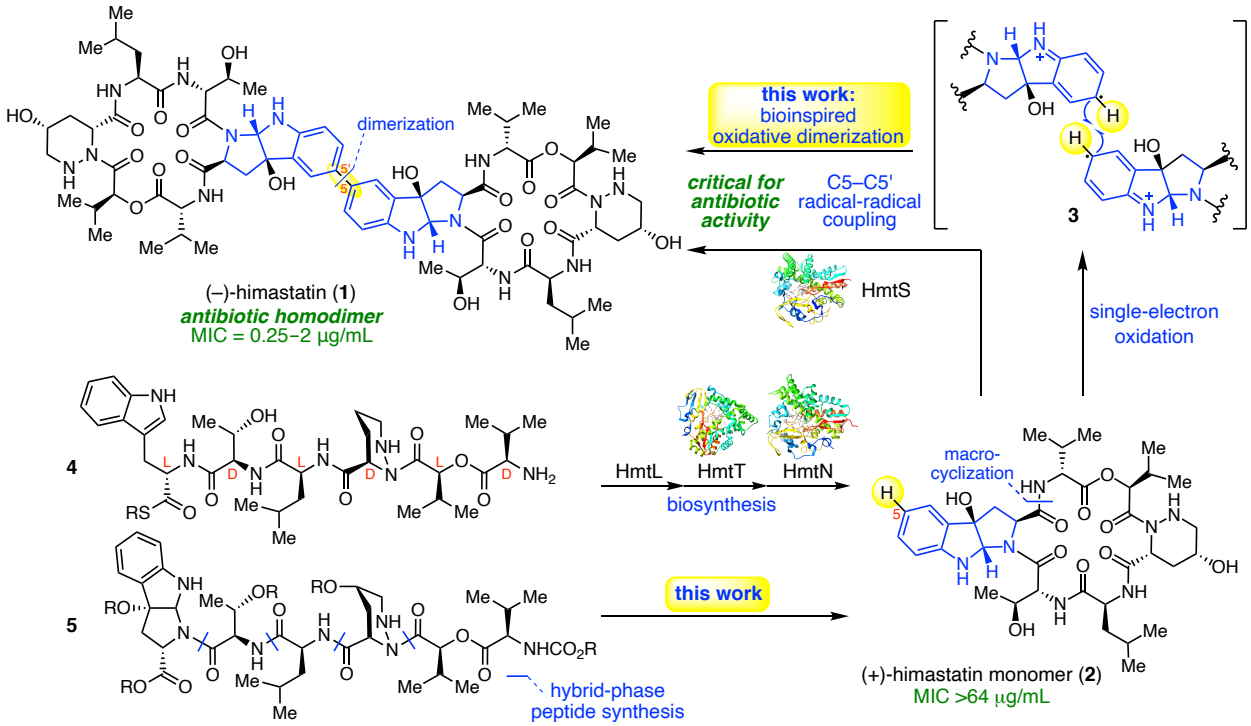

Fig. 1. Comparison of the biogenesis of himastatin and our bioinspired synthetic strategy. MIC values for (–)-himastatin (**1**) are taken from ref. 4 against Gram-positive bacteria. MIC = minimum inhibitory concentration.

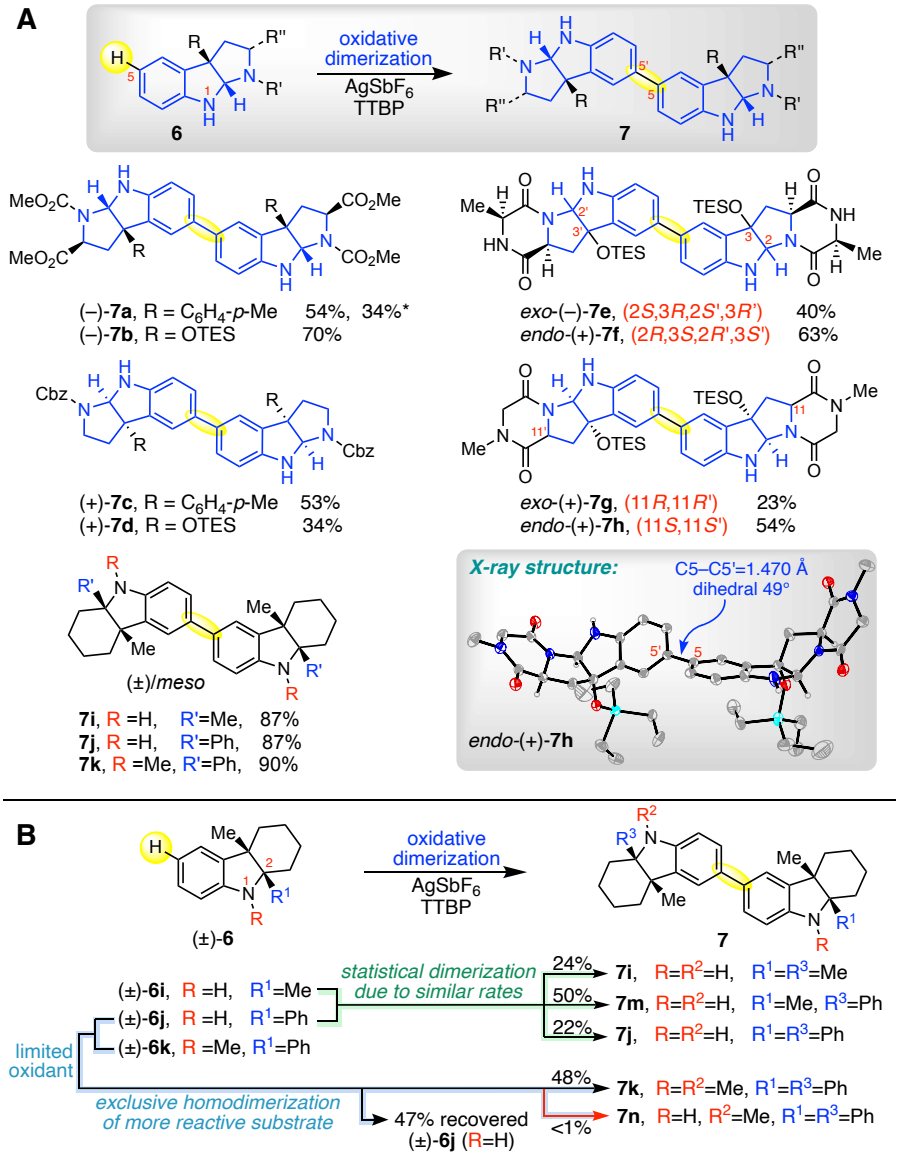

Fig. 2. Oxidative Dimerization of Cyclotryptophan, Cyclotryptamine, and Indolines. (**A**) Substrate scope of our oxidative dimerization reaction. In the ORTEP representation of dimeric *endo*-diketopiperazine (+)-**7h**, the thermal ellipsoids are drawn at 30% probability and only selected hydrogen atoms are shown. (**B**) Mechanistic studies using equimolar mixtures of differentially substituted indolines provide evidence for a radical–radical coupling mechanism. Reagents and conditions: $AgSbF_6$, TTBP, $ClCH_2CH_2Cl$, 23 °C; * Copper(II)-catalyzed conditions: $Cu(OTf)_2$ (20 mol%), Ag_2CO_3, $ClCH_2CH_2Cl$, 23 °C. TES = triethylsilyl; TTBP = 2,4,6-tri-*tert*-butylpyrimidine.

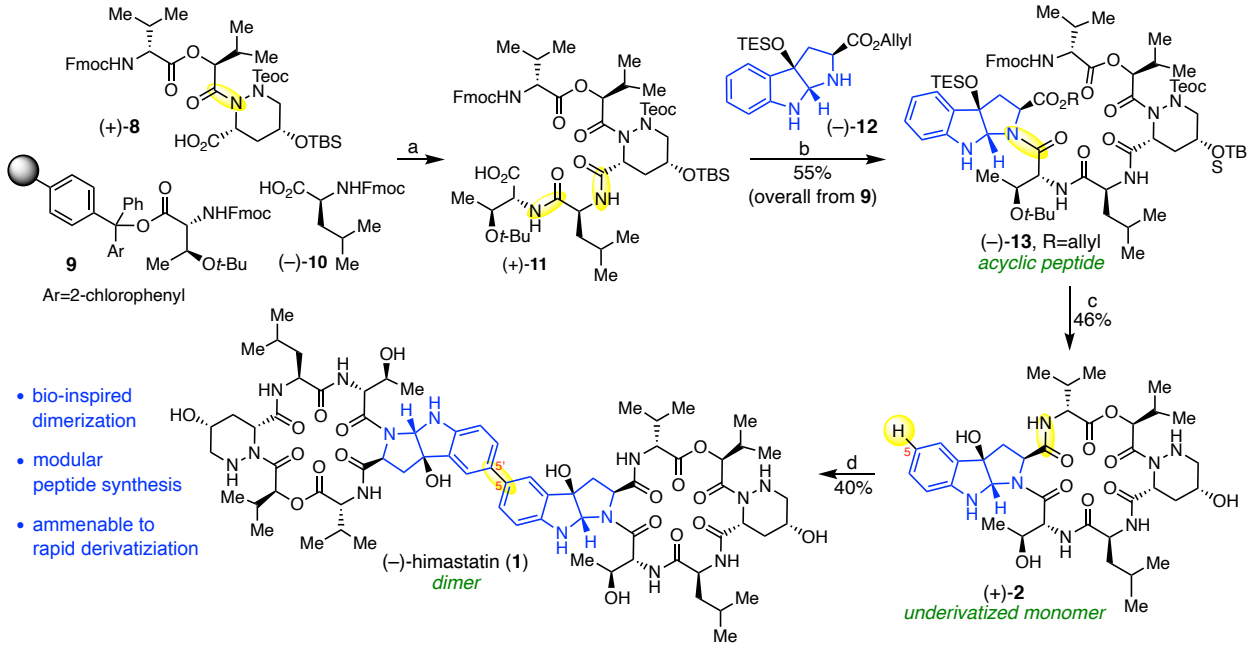

Fig. 3. Concise total synthesis of (–)-himastatin (1). Reagents and conditions: (a) (i) piperidine, DMF, 23 ºC, (ii) (–)-**10**, HATU, *i*-Pr_2NEt, DMF, 23 ºC, (iii) piperidine, DMF, 23 ºC, (iv) (+)-**8**, HATU, *i*-Pr_2NEt, DMF, 23 ºC, (v) TFA, CH_2Cl_2, 23 ºC; (b) (–)-**12**, HATU, HOAt, 2,4,6-collidine, CH_2Cl_2, 0 → 23 ºC; (c) (i) $Pd(PPh_3)_4$, *N*-methylaniline, THF, 23 ºC, (ii) *i*-Pr_2NH, MeCN, 23 ºC, (iii) HATU, HOAt, *i*-Pr_2NEt, CH_2Cl_2, 23 ºC, (iv) TFA, H_2O, anisole; Et_3N, MeOH, 23 ºC; (d) $Cu(SbF_6)_2$, DTBMP, $ClCH_2CH_2Cl$, 23 °C. Ar = 2-chlorophenyl; DMF = *N,N*-dimethylformamide; DTBMP = 2,6-di-*tert*-butyl-4-methylpyridine; Fmoc = 9-fluorenylmethoxycarbonyl; HATU = hexafluorophosphate azabenzotriazole tetramethyl uronium; HOAt = 1-hydroxy-7-azabenzotriazole; Leu = Leucine; TBS = *tert*-butyldimethylsilyl; Teoc = 2-trimethylsilylethyloxycarbonyl; TFA = trifluoroacetic acid; THF = tetrahydrofuran.

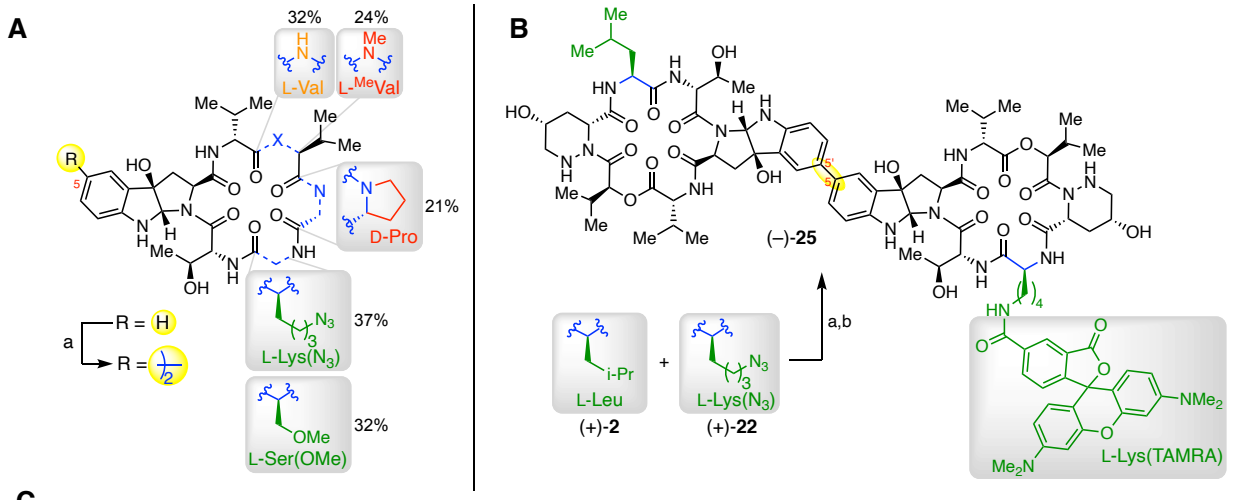

C

compound	*monomer*	**MIC** (μg/mL) ***B. subtilis***	*dimer*	***B. subtilis***	**MRSA**	**MSSA**	**VRE** ***faecalis***	**VSE** ***faecalis***	***S. himastatinicus*** ***(producing organism)***
				MIC (μg/mL)					
(–)-himastatin	(+)-**2**	>64	(–)-**1**	1	2	1	1	1	8
ent-(+)-himastatin	(–)-**2**	>64	(+)-**1**	0.5	2	2	2	1	1
meso-himastatin	-	-	*meso*-**1** ***heterodimer***	1	2	1	1	1	4
rac-himastatin	(±)-**2**	>64	(±)-**1**	0.5	2	2	1	1	2
single-residue substitutions									
L-Val	(+)-**14**	>64	(–)-**15**	8	64	16	32	16	>64
L-^{Me}Val	(+)-**16**	>64	(–)-**17**	>64	>64	>64	>64	>64	>64
D-Pro	(+)-**18**	>64	(–)-**19**	>64	>64	>64	>64	>64	>64
L-Ser(OMe)	(+)-**20**	>64	(–)-**21**	2	4	4	1	2	8
L-Lys(N_3)	(+)-**22**	>64	(–)-**23**	2	2	2	2	1	8
L-Lys(TAMRA)	(–)-**24**	>64	(–)-**25** ***heterodimer***	6	>64	>64	16	16	-

Fig. 4. Designed derivatives and probes of himastatin reveal critical structural elements for antibiotic activity. (**A**) Dimerization of unnatural himastatin derivatives with single-residue substitutions. (**B**) Synthesis of a heterodimeric fluorescent himastatin probe. (**C**) Antibiotic evaluation of himastatin derivatives and probes against Gram-positive bacteria. MIC values were determined using the broth-microdilution method; see Table S10. Reagents and conditions: (a) $Cu(SbF_6)_2$, DTBMP, $ClCH_2CH_2Cl$, 23 °C; (b) (i) PMe_3, H_2O, THF, 40 °C, (ii) 5-TAMRA succinimidyl ester, *i*-Pr_2NEt, DMF, 23 ºC. Lys = lysine; MRSA = methicillin-resistant *Staphylococcus aureus*; MSSA = methicillin-sensitive *S. aureus*; Pro = proline; Ser = serine; TAMRA = carboxytetramethylrhodamine; Val = Valine; VRE = vancomycin-resistant *Enterococcus;* VSE = vancomycin-sensitive *Enterococcus*.